Bioactive Materials 26 (2023) 77–87

Contents lists available at ScienceDirect

Bioactive Materials

journal homepage: www.keaipublishing.com/en/journals/bioactive-materials

3D-printed fish gelatin scaffolds for cartilage tissue engineering

Abudureheman Maihemuti [a,b], Han Zhang [d], Xiang Lin [d], Yangyufan Wang [a,b], Zhihong Xu [a,b,**], Dagan Zhang [e,***], Qing Jiang [a,b,c,*]

[a] State Key Laboratory of Pharmaceutical Biotechnology, Division of Sports Medicine and Adult Reconstructive Surgery, Department of Orthopedic Surgery, Nanjing Drum Tower Hospital, The Affiliated Hospital of Nanjing University Medical School, 321 Zhongshan Road, Nanjing, 210008, Jiangsu, PR China
[b] Branch of National Clinical Research Center for Orthopedics, Sports Medicine and Rehabilitation, PR China
[c] Co-innovation Center of Neuroregeneration, Nantong University, PR China
[d] Department of Rheumatology and Immunology, Nanjing Drum Tower Hospital, School of Biological Science and Medical Engineering, Southeast University, Nanjing, 210096, PR China
[e] Department of Rheumatology and Immunology, Institute of Translational Medicine, The Affiliated Drum Tower Hospital of Nanjing University Medical School, Nanjing, 210002, PR China

ARTICLE INFO

Keywords:
3D printing
Fish skin gelatin
Sodium alginate
Cartilage defect repair
Tissue engineering

ABSTRACT

Knee osteoarthritis is a chronic disease caused by the deterioration of the knee joint due to various factors such as aging, trauma, and obesity, and the nonrenewable nature of the injured cartilage makes the treatment of osteoarthritis challenging. Here, we present a three-dimensional (3D) printed porous multilayer scaffold based on cold-water fish skin gelatin for osteoarticular cartilage regeneration. To make the scaffold, cold-water fish skin gelatin was combined with sodium alginate to increase viscosity, printability, and mechanical strength, and the hybrid hydrogel was printed according to a pre-designed specific structure using 3D printing technology. Then, the printed scaffolds underwent a double-crosslinking process to enhance their mechanical strength even further. These scaffolds mimic the structure of the original cartilage network in a way that allows chondrocytes to adhere, proliferate, and communicate with each other, transport nutrients, and prevent further damage to the joint. More importantly, we found that cold-water fish gelatin scaffolds were nonimmunogenic, nontoxic, and biodegradable. We also implanted the scaffold into defective rat cartilage for 12 weeks and achieved satisfactory repair results in this animal model. Thus, cold-water fish skin gelatin scaffolds may have broad application potential in regenerative medicine.

1. Introduction

Knee osteoarthritis is one of the most common degenerative diseases of middle-aged and elderly patients [1–3]. As the disease progresses, localized cartilage injuries with obtuse edges develop into areas of cartilage defect. Since there are no blood vessels in articular cartilage, nutrients have difficulty reaching these areas, which leads to a slow rate of cartilage self-repair or even no recovery at all [4–6]. Currently, commonly used treatment methods include intra-articular injections, microfracture, autologous cartilage or stem cell transplantation, platelet-rich plasma, and scaffold-assisted technology [7–11]. Among these, scaffold-assisted technology is considered by many researchers to have excellent application prospects [12–14]. The presence of scaffolds can better fill the injured area than other methods, and the absence of scaffolds may lead to cell dissociation [15,16]. In addition, this method typically involves fewer complications and shorter postoperative recovery times [17,18]. Furthermore, the cells in the scaffold are less likely to dedifferentiate and more likely to form hyaline cartilage as the scaffold mimic the extracellular matrix like microstructure of bone-like tissues [19,20]. Based on these advantages, suitable scaffold materials

Peer review under responsibility of KeAi Communications Co., Ltd.
* Corresponding author. State Key Laboratory of Pharmaceutical Biotechnology, Division of Sports Medicine and Adult Reconstructive Surgery, Department of Orthopedic Surgery, Nanjing Drum Tower Hospital, The Affiliated Hospital of Nanjing University Medical School, 321 Zhongshan Road, Nanjing, 210008, Jiangsu, PR China.
** Corresponding author. Branch of National Clinical Research Center for Orthopedics, Sports Medicine and Rehabilitation, PR China.
*** Corresponding author.
E-mail addresses: xuzhihong@njglyy.com (Z. Xu), zhangdagan@126.com (D. Zhang), qingj@nju.edu.cn (Q. Jiang).

https://doi.org/10.1016/j.bioactmat.2023.02.007
Received 20 October 2022; Received in revised form 20 January 2023; Accepted 8 February 2023

that can load cells effectively and promote cartilage defect repair are highly anticipated [21–26].

Here, we propose a novel 3D-printed scaffold for cartilage defect repair. Compared with bone tissue engineering scaffolds made using other technologies, cartilage scaffolds prepared by 3D printing have unique advantages in scaffold personalization, accuracy, mechanical strength, pore adjustment, and spatial structure complexity [27–32]. Current studies have found that 3D-printed cartilage tissue engineering scaffolds also have the advantages of high porosity, uniform pore distribution, high pore connectivity, and compressive strength [33]. Moreover, many hydrogel scaffolds have good cytocompatibility, which has a pronounced promoting effect on cartilage repair [34–38]. Hydrogel materials are formed by cross-linking hydrophilic polymers through covalent bonds or physical attraction. They also absorb water and swell, making them more porous and permeable, facilitating cell migration and efficient transport of oxygen and nutrient molecules [39]. Once swollen, a hydrogel provides enough space for cells to proliferate and grow within its matrix [40–43]. However, many chemically synthesized hydrogels require substantial capital investment to create and extreme polymerization conditions, leading to uncertain bio-toxicity [44–46]. More importantly, these hydrogels lack the necessary conditions to mimic the extracellular matrix microenvironment [47,48]. Therefore, there is an urgent need to develop naturally derived hydrogel materials for cartilage tissue engineering [49–51].

In this study, we used natural gelatin extracted from cold-water fish skin, mixed with sodium alginate hydrogel to 3D print a hydrogel scaffold for repairing knee cartilage defects (Fig. 1). Due to the low viscosity of the cold-water fish skin gelatin solution at room temperature, natural sodium alginate hydrogel was used to increase the viscosity of the printed pre-gel and formed an interpenetrating double-network hydrogel structure. The addition of sodium alginate made the 3D-printed cartilage scaffold's shape more controllable, its mechanical strength more in line with practical application requirements, and insusceptible to the rapid degradability of fish gelatin *in vivo*. In addition, the micropores of the 3D-printed scaffolds were interconnected and evenly distributed, which can better simulate the extracellular matrix, give cells more support points, and facilitate the exchange of nutrients and signals between cells. These excellent properties provide an ideal environment for the growth of cartilage-like tissues so that fish gelatin 3D-printed scaffolds can effectively promote the repair rate of cartilage and become a promising new method for cartilage tissue engineering.

2. Results and discussion

Cold-water fish skin contains collagen and has low immunogenicity, so the natural gelatin extracted from it can be used as an ideal scaffold material for repairing cartilage defects. Since the cold-water fish skin gelatin solution has low viscosity at room temperature, we mixed it with sodium alginate to prepare biomaterial ink for preparing shape-stable 3D scaffolds. $CaCl_2$ and EDC-NHS were used for crosslinking sodium alginate and fish skin gelatin to maintain its specific design patterns and prevent it from melting at room temperature. The rheological properties and shear rates of pure gelatin, pure sodium alginate, and fish skin gelatin/sodium alginate hybrids were also measured to find the correct viscosity and concentration that extrusion-type 3D printing equipment could print.

Different percent weight-in-volume ratios (% W/V) of biomaterial inks, such as 6% sodium alginate (G0A6), 15% cold-water fish skin gelatin (G15A0), 15/3% fish gelatin/sodium alginate (G15A3), and 15/6% fish gelatin/sodium alginate (G15A6) exhibited different flow behaviors (Fig. 2a). Pure cold-water fish skin gelatin was liquid at room temperature, and could completely flow into the bottom of its bottle after 15 min, but the components of cold-water fish skin gelatin and sodium alginate (G15A3, G15A6, and G15A10) could not wholly flow into the bottom of the bottle. This clearly showed that the addition of sodium alginate significantly increased the viscosity of the gelatin. We also observed that the compositional thickness of the mixed biomaterial ink groups had a much higher viscosity than pure cold-water fish skin gelatin (Fig. 2b). Thus, cold-water fish skin gelatin/sodium alginate mixture groups had better shear-thinning behavior, which meant that they could be easily extruded from the nozzle of an extrusion-type 3D printer.

In addition, we also tested the mixtures' shear moduli G′ and G″-angular frequency (Fig. 2c, Fig. S1) and found that the G15A10 group had the highest shear modulus and that the G15A0 group had the lowest, which we attributed to sodium alginate. The storage moduli G′ of each compositional group was higher than the loss moduli G″ as well, indicating that the synthesized biomaterial was a relatively stable gel after a short period of time. However, the G′ and G″ relationship of pure cold-water fish skin gelatin (Fig. S1) was irregular and liquid.

We further investigated the suitable % W/V for printing cold-water fish skin gelatin and sodium alginate by testing a series of different % W/V ink compositions (Fig. 2d) and found out that the % W/V of G15A6

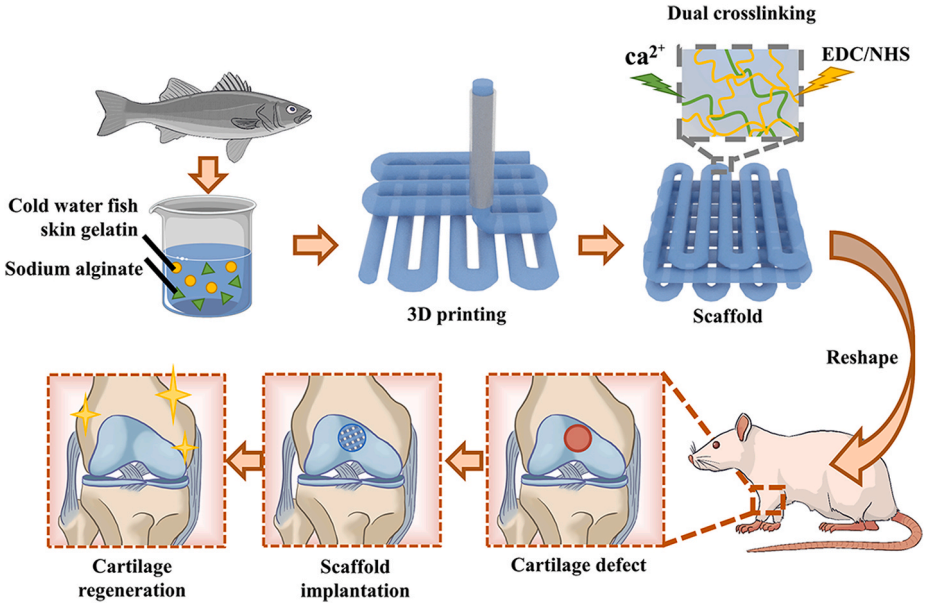

Fig. 1. Scheme of 3D-printed cold-water fish skin gelatin scaffolds for cartilage tissue regeneration.

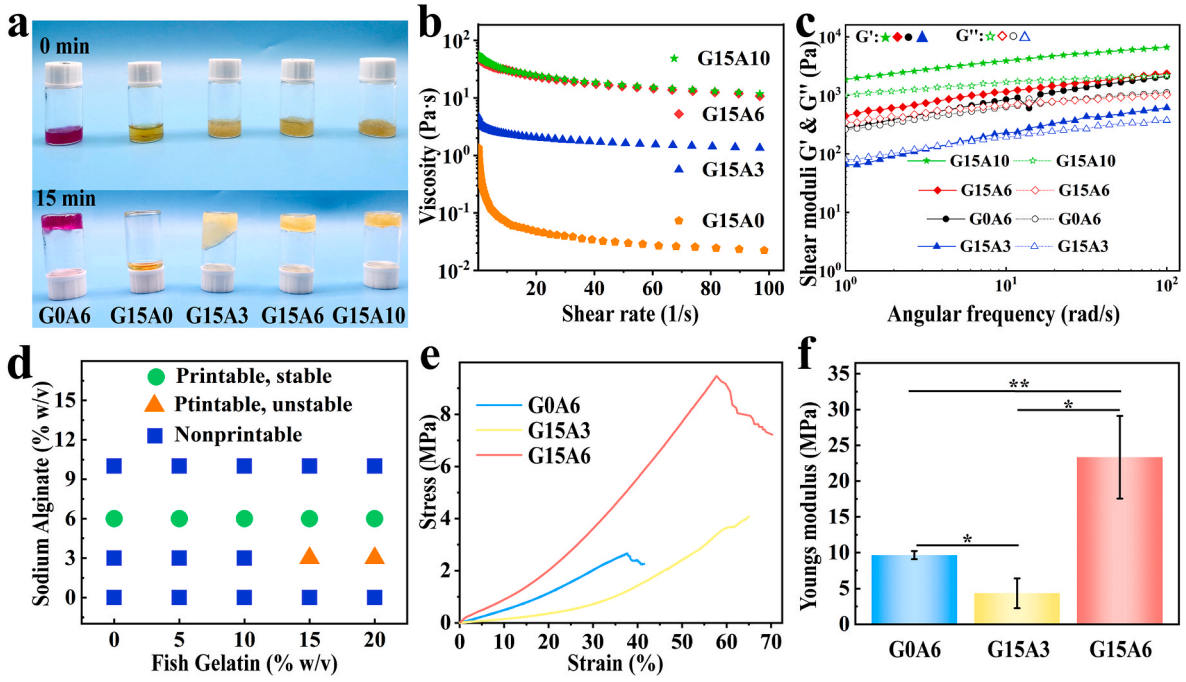

Fig. 2. Rheological and mechanical properties of the fish gelatin/sodium alginate inks: (a) flow behavior; (b) viscosity-shear rate; (c) shear moduli-angular frequency; (d) printability tested by a series of different % W/V ink compositions; (e) stress-strain; (f) Young's modulus of the respective biomaterial inks with different % W/V; G0A6: 6% sodium alginate, G15A0: 15% fish skin gelatin, G15A3: 15/3% fish gelatin/sodium alginate, G15A6: 15/6% fish gelatin/sodium alginate, G15A10: 15/10% fish gelatin/sodium alginat.

could be printed smoothly and could hold its shape before crosslinking. In fact, the composition of biomaterial ink was printable and stable only when it included 6% sodium alginate, as this kept the viscosity in a printable range that was neither too high to extrude nor too low to stay in shape. These results were further checked by 3D printing the abbreviation of Nanjing University ("NJU") with biomaterial inks containing different ratios of sodium alginate, and we found the result to be the best with % W/V of G15A6. The materials were either too diluted to make a clear, accurate pattern or too viscous to print fluently at other ratios (Fig. S2).

As Fig. 2e shows, the compressive stress-strain curves of the three mixtures of fish skin gelatin/sodium alginate ink were all within a certain range. They exhibited linear stress-strain behavior, and the stress-strain performance of the G15A6 group was the best, demonstrating both better elasticity and compressive capacity. The Young's modulus calculated from the stress-strain data (Fig. 2f) also showed that the G15A6 group stood out among the groups, indicating that the % W/V of G15A6 could be used as a suitable ratio for printing weight-bearing organs such as knee joints.

In extrusion 3D printing, parameters such as the % W/V of the biomaterial ink, the diameter of the printing nozzle, the air pressure, and the printing speed all impact the printing process. In addition, the distance between the filaments, the thickness of each layer, and the crossing angle can also be changed by adjusting different parameters. Therefore, we selected some key parameters and studied the effects of different settings on the printing results. As presented in Fig. S3, the filament diameter D increased with the increase of the nozzle diameter D, but it did not match precisely because the hydrogels had a certain die-swelling effect, and when the nozzle diameter was fixed (25G: 250 μm), the filament diameter D increased with air pressure P (Fig. S3d). After determining the appropriate % W/V combination (G0/A6, G15/A3, or G15/A6) for biomaterial inks, we used parameters such as 25G for nozzle diameter, air pressure of 0.2 MPa, printing speed of 10 mm/s, a cylinder-shaped model, printed several scaffolds, crosslinked and observed both macroscopically and microscopically.

Fig. 3a shows optical microscopic photos of the G15/A6 scaffolds after printing (Fig. 3a I), then crosslinking and freeze-drying (Fig. 3a II), and crosslinking and drying at room temperature (Fig. 3a III). Fig. 3b (I, II) showed that the microstructures of the scaffolds were regular and evenly distributed at different parts of the scaffolds. It can be seen from Fig. 3bIII that the scaffolds had high porosity, which makes them convenient for nutrient transport and interconnections between cells, and also provides space for cell adherence. Due to the shape controllability of 3D printing technology, we were able to print 3D scaffolds with many different shapes, such as NJU (the abbreviations of Nanjing University) (Fig. 3c I, II), hexagons (Fig. 3c III), flowers (Fig. 3c IV), snowflakes (Fig. 3c V), index fingers (Fig. 3c VI), and other patterns.

To test the feasibility of scaffold implantation *in vivo*, we began by examining the scaffold's biocompatibility. Due to the excellent biocompatibility of cold-water fish skin gelatin and mixed hydrogel, the fluorescence microscope images (Fig. S4a) and CCK8 experiments (Fig. S4b) of the C28 cells cultured with scaffold immersed mediums showed good morphology after 3 days. According to our cell co-culture (Fig. 4a) and its quantification (Fig. S5) results, the 15/6% fish gelatin/sodium alginate (GA) group scaffold had the highest cell proliferation effect, with 5/6% fish gelatin/sodium alginate scaffold group ranking second. The 6% sodium alginate (A) group had less cell proliferation than the other groups. Moreover, the cell proliferation effect was increased with cold-water fish skin gelatin content, which suggests the outstanding biocompatibility of cold-water fish skin gelatin (Fig. 4a). These results also agreed with cell growth effect of CCK8 experiments (Fig. 4c). Therefore, these consistent results suggest that cold-water fish skin scaffolds have good biosafety properties.

When C28 cells were grown on a 3D scaffold, overlapping growth could be achieved due to the multi-layer structure of the scaffold, which is impossible on ordinary Petri dishes. Besides, primary chondrocytes cultured on the scaffolds almost filled the pores of the scaffolds during the 21 days of growth (Fig. 4b II, III). In addition, the optic microscopic image of the phalloidin staining of the different parts of the scaffolds seeded with C28 cells (Fig. 4b I, S6) also indicated good biocompatibility. Furthermore, the overlapping growth of cells was relatively uniform in different parts of the scaffold, which may be a potential

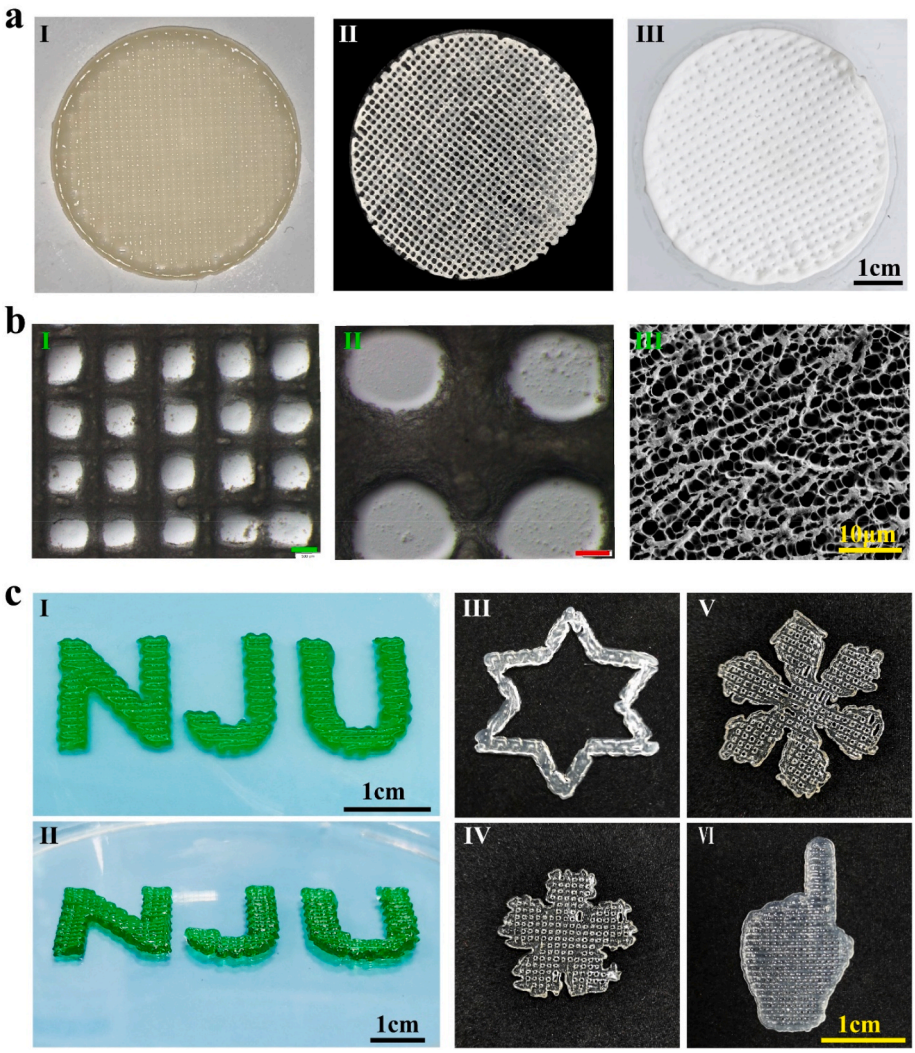

Fig. 3. Macro and micro views of the 3D-printed scaffolds: 3D-printed scaffolds, after crosslinking (a I), freeze-dried (a II), crosslinked and dried at room temperature (a III); stereo microscopic (b I-II) and SEM (b III) image of the scaffolds (scale bars: green: 500 μm, red: 200 μm); (c) front and side views (c I-II) of " NJU ", the abbreviation of Nanjing University, various kinds of shapes (c III-VI). All scaffolds above were 3D-printed with 15/6% fish gelatin/sodium alginate biomaterial ink.

breakthrough for generating multilayer cartilage structures to repair defective tissue **(**Video S1**)**. Western blot analysis (Fig. 4d and e) showed that the expressions of Collagen II, Aggrecan, and Sox9 on the GA group scaffolds were much better than those in the other two groups, and this result was statistically significant. The results above were also obtained from the relative mRNA expression (Fig. 4f, g, h) of C28 cells cultured on three plates (see Table S1 for qPCR primers).

Many biomaterials have immunogenicity problems. To study the immunogenicity of our biomaterial inks, biomaterial inks that had been crosslinked with Ca^{2+} and EDC/NHS were implanted subcutaneously in mice, as displayed in Fig. 5a, **b** and **S6**. As expected, H&E staining didn't manifest obvious inflammatory cell infiltration (Fig. 5a), and the counts and percentages of WBC, LYM, MON, and N (Fig. 5b) also fell within the normal range, meaning that the biomaterial inks didn't trigger inflammation. Additionally, there were no significant changes in markers for hemopoietic functions such as WBC, RBC, and PLT (Fig. 5a, Fig. S7a), markers of liver function (ALT, AST, ALB, and γ-GT), or markers of kidney function (UREA) (Fig. S7 b). These results indicated that our scaffolds didn't cause immunological rejection, which was further borne out by H&E staining of major organs and blood biochemistry analysis (Fig. S8) of rats 3 months after scaffold implantation for knee cartilage defect repair.

To investigate the biodegradability of the scaffolds, we performed *in vitro* and *in vivo* degradation experiments. As the small-animal imaging of the rats (Fig. 5c) and its statistical analysis (Fig. 5e) showed, G group biomaterials had already completely degraded at 27 days, while A group scaffolds fully degraded at 35 days and mixed GA scaffolds at 32 days. These results were likely due to the biogenic and collagen-rich features of the fish skin gelatin as rats also contain collagenase that can accelerate the scaffolds' degradation at body temperature. Moreover, 1 month is enough to activate the self-growing and self-repairing mechanism for cartilage and bone-tissue to some extent. In addition, relative fluorescence intensity analysis of the small-animal images supported the results demonstrated above (Fig. S9). We also put the same kinds of scaffolds into culturing dishes and included alginate lyase for A group scaffolds, collagenase type I for G group scaffolds, and both of these enzymes for GA group scaffolds, and they dissolved at 14, 9, and 12 days, respectively, *in vitro* at 37 °C (Fig. 5d). This was because appropriate enzymes and ideal temperatures accelerated the dissolving of the scaffolds. Thus, we determined that our scaffolds are safe for animal experiments by several important metrics.

In order to ascertain the practical application effects of the 3D scaffolds, we studied the repair effect of the scaffolds in SD rat knee articular cartilage defect models (Fig. 6). Cartilage repair effects were observed and scored by the International Cartilage Repair Society (ICRS) cartilage lesion classification system (Fig. 6b, d and Table S2). To

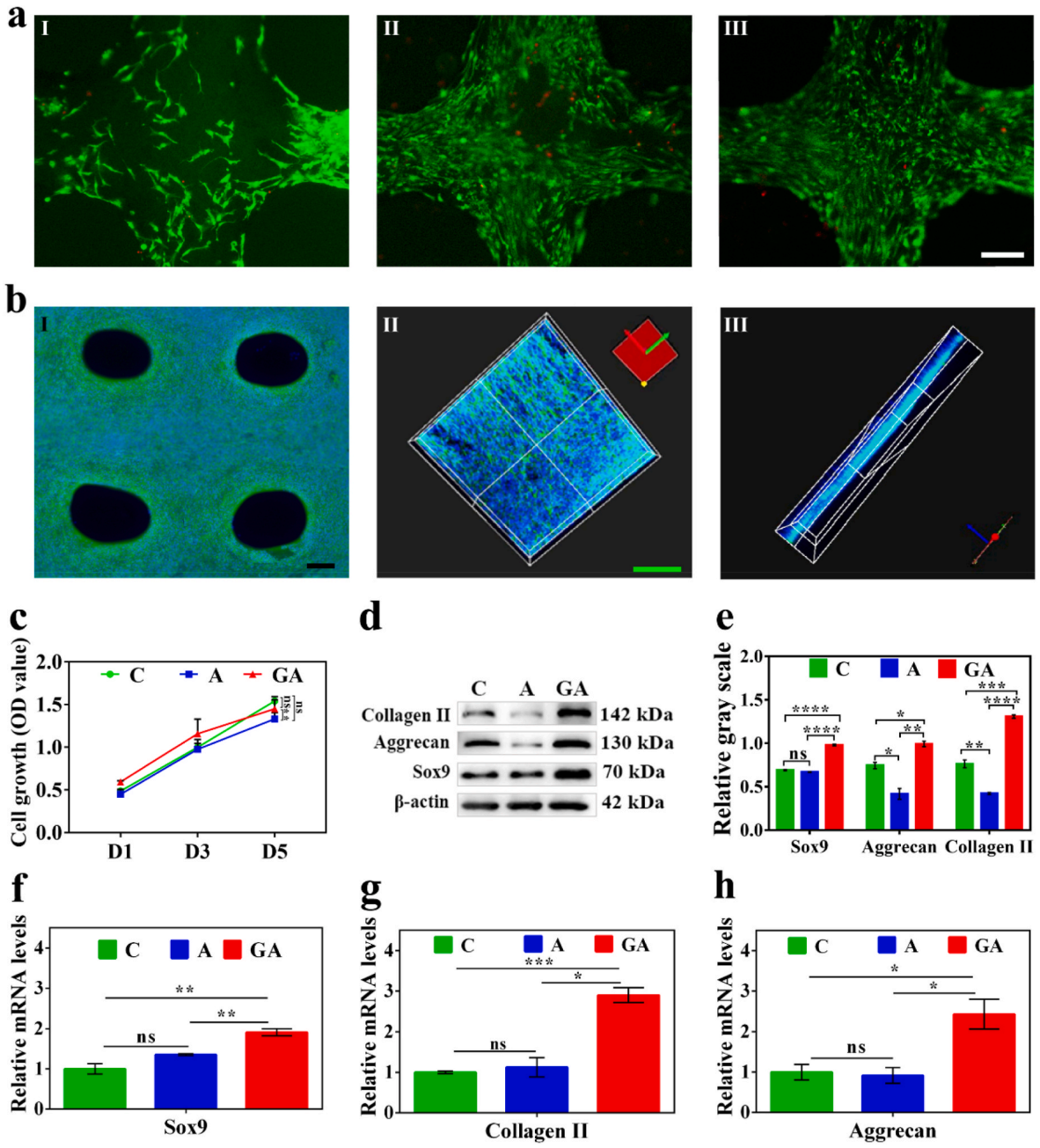

Fig. 4. Evaluation of the biocompatibility of the 3D-printed fish gelatin scaffolds: (a) FDA/PI staining of C28 cells cultured on the 3D-printed scaffolds for 5 days, 6% sodium alginate (a I), 5/6% fish gelatin/sodium alginate (a II), and 15/6% fish gelatin/sodium alginate (a III) scaffolds; Phalloidin and DAPI staining of cells co-cultured on the 15/6% fish gelatin/sodium alginate (GA) scaffolds: (b I) fluorescence microscopic images of C28 cells cultured for 7days and (b II, III) confocal microscopic images of the primary chondrocytes cultured for 21 days; (c) the cell growth (OD value) of C28 cells cultured on C, A, and GA scaffolds for 5 days; western blot analysis (d) and relative gray scale (n = 3) (e) of Collagen II, Aggrecan, and SOX9 of the C28 cells cultured on the C, A, and GA scaffolds for 5 days; relative mRNA levels (n = 3) of SOX9 (f), Collagen II (g), and Aggrecan (h) of the C28 cells cultured on the C, A, and GA scaffolds for 5 days. C: control; A: 6% sodium alginate; GA: 15/6% fish gelatin/sodium alginate; scale bars: white (a I) - (a III) 100 μm, black (b I) 200 μm, green (b II) - (b III) 50 μm, $p < 0.05$.

observe the degree of articular cartilage repair, we performed magnetic resonance imaging (MRI) of the knee joint on harvested rat knees at 3 months (Fig. 6c). Due to the excellent biocompatibility of the 3D-printed scaffolds and the presence of vital collagen for repairing cartilage defects, the GA group almost completely repaired the hole with a smooth surface, but the A group had noticeable defect holes and lines with a rough surface, as indicated by the red arrows and circles (Fig. 6b and c). In contrast, the holes of the control group were deep and clear. Intermittent low-intensity lines, possibly regenerated cartilage, could also be observed on MRI pictures. However, the holes in groups C and A had been filled with soft tissue. Moreover, no signs of fluid accumulation or inflammation were seen in any group of knee MRI images. We also measured the cartilage defect area based on the MRI images of each group, obtained the same results, and found a statistical difference between the three groups (Fig. 6e).

After three months of *in vivo* implantation, the rats were euthanized, and the knee joints were taken out for histological analysis (Fig. 7) to observe the effects of treatment. Although the overall treatment effects of the full-thickness cartilage defect of the GA and A groups were limited, we gained some promising results. As the H&E staining in Fig. 7a shows, the GA group had more regenerated cartilage than the A and C groups, and the A group also had a layer of cartilage. Moreover, no

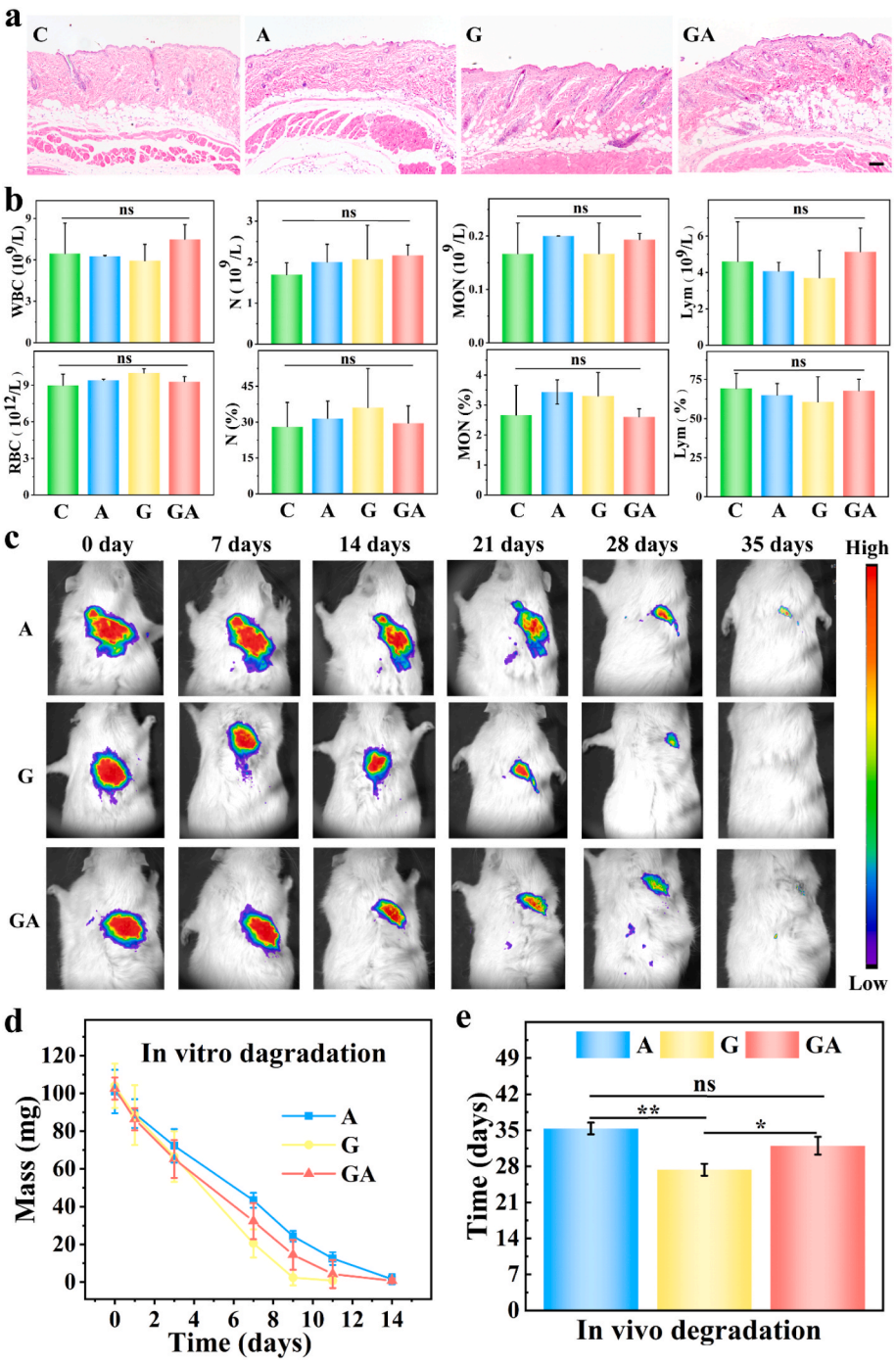

Fig. 5. Evaluation of immunogenicity (a)–(b) and degradation (c)–(e) of the biomaterial inks and scaffolds: H&E staining of the skin (a) and routine blood examination (b) of mice implanted with or without crosslinked biomaterial inks for 2 weeks (n = 4); examined parameters including white blood cell (WBC) count, red blood cell (RBC) count, lymphocyte (LYM), monocyte (MON), neutrophils (N) and their percentages; (c) small-animal imaging of the rats implanted with three kinds of Cy7 labeled biomaterials for 37days (n = 5); (d) *in vitro* degradation of the biomaterials immersed in enzymes for 2 weeks (n = 3); (e) quantification of small-animal imaging (c) (n = 3); (C: control, A: 6% sodium alginate 3D-printed scaffolds crosslinked with Ca^{2+}, G: 15% cold-water fish skin gelatin crosslinked with EDC/NHS, GA: 15/6% fish gelatin/sodium alginate 3D-printed scaffolds crosslinked with Ca^{2+} and EDC/NHS). The scale bar is 100 μm.

inflammatory cell infiltration was found from the highly magnified views of the H&E staining (Fig. S10). However, the holes in the control group had been filled with irregular fibrous tissue. We counted the relative DNA content (Fig. 7b) and found that the number of cells in the GA group was much higher than that in the A and C groups. As shown in Fig. 7a, we also performed Masson staining to investigate collagen content and Safranin O-Fast Green staining to understand cartilage and bone growth, and found that the GA group had the best collagen content and quality of regenerated cartilage compared to other groups. Statistical analysis of relative collagen content and relative GAG content (Fig. 7b) also showed that the GA scaffolds had a significant therapeutic effect compared to the A and C groups.

We also carried out Elisa (Fig. 7c) and immunofluorescence staining (Fig. 7e) of representative collagen II (COL2) and Aggrecan (ACAN) for the different groups. Because of the collagen content in the GA group, we could see clearly that the GA group had more collagen (II) and Aggrecan content than the C and A groups (Fig. 7c). Statistical analysis also demonstrated the same results and showed a statistically significant difference between groups (Fig. 7d). We further investigated specific markers of regenerated cartilage, Collagen II, and Aggrecan (Fig. 7e) by immunofluorescence staining and found that both Aggrecan and Collagen II existed primarily at the dense area of regenerated cartilage but were especially highly expressed in the GA group. Once again, our statistical analysis gave the same results and showed that there were statistically significant differences between groups (Fig. 7f). Thus, we conclude that cold-water fish skin gelatin and sodium alginate hybrid scaffolds are effective in repairing injured cartilage of the knee joint.

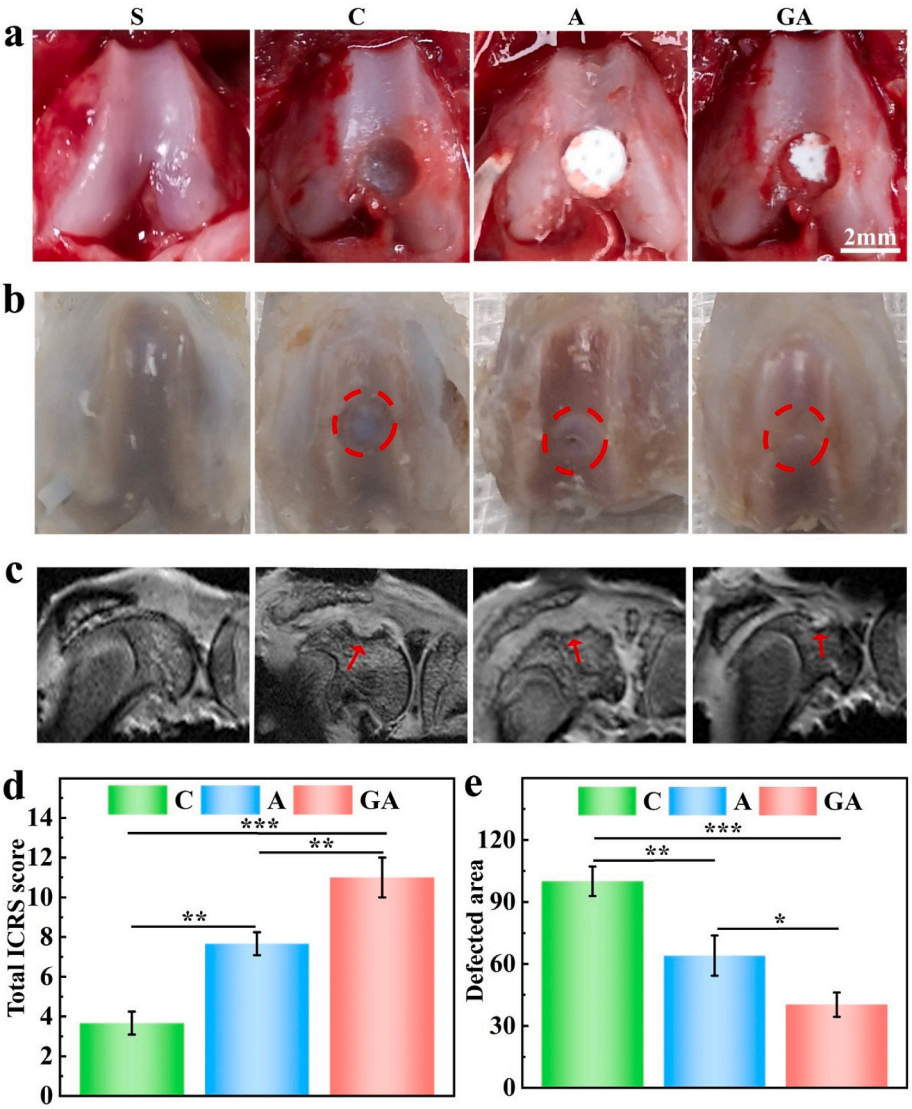

Fig. 6. Gross view and MRI image of the animal experiment (n = 5): (a) the creation of the rat knee cartilage defect model; (b) 3 months after implantation; (c) MRI of harvested knee joints of the rats at 3 months after implantation; (d) the statistical analysis of the Total ICRS score of the three groups; (e) the quantification and statistical analysis of the defected areas in MRI images. the groups were S (sham), C (control), A (6% sodium alginate scaffold), and GA (15%/6% fish gelatin/sodium alginate scaffold). The red circles in (b) demonstrate the initial range of the holes; the red arrows in (c) point to the defected part of the repaired holes.

3. Conclusions

In this research, we prepared cold-water fish skin gelatin scaffolds as biodegradable, biocompatible, low immunogenic, and free from religious problems and zoonotic diseases caused by porcine gelatin. We further investigated appropriate percent W/V of bio-inks, 3D printed various kinds of scaffolds and used optimized 3D scaffolds to repair knee articular cartilage defects. The experimental results show that the scaffold can simulate the extracellular environment of bone-like tissue and has multiporous, uniformly distributed, interconnected, and multilayer structures inside. In addition, the mechanical properties, cytotoxicity, immunogenicity, and degradability of the scaffolds were studied and tested. In animal experiments, the optimized scaffolds successfully repaired the defected cartilage.

Here, we propose a biodegradable and low immunogenicity biomaterial that does not contain mammalian pathogens and also provide an idea to simulate the natural structure of bone-like tissue: the structure of Haversian tube by using porous scaffolds. Although our scaffolds are promising in cartilage defect repair, their repairing effect on rat knee cartilage defects is limited. The scaffolds need to be cross-linked to make them stable at room temperature, and they are still not ideal for completely replacing bone tissue *in vivo*. In order to achieve better repair effects and accelerate the healing process, the scaffolds can further load cells, exosomes, cytokines, and encapsulate drugs. In addition, the scaffolds may be able to replace an injured meniscus after modification and provide nutrition for the injured knee joint simultaneously. Therefore, 3D printing hydrogel made of cold-water fish skin gelatin may become an ideal product for cartilage regeneration, which is a promising topic and deserves further research.

4. Methods

Materials: Gelatin from cold-water fish skin (G7041 1-100G) and sodium alginate (medium viscosity, average Mw80,000 –120,000, M/G ratio 1.56) were purchased from Sigma Aldrich, USA; 1-ethyl-3-(3-dimethylaminopropyl) carbodiimide hydrochloride (EDC), N-hydroxysuccinimide (NHS) were acquired from Proteochem (Denver, CO); C28 cells came from the Chinese Academy of Sciences (Shanghai, China). DMEM high glucose culture medium (319-006-CL) was bought from WESENT CORPORATION, Nanjing, China. Additionally, SYBR Qpcr SuperMix plus(E096) was bought from Novoprotein, Shanghai, China. 2xTaq Master Mix (Dye Plus) (P112-01) was bought from Vazyme, Nanjing, China. Annexin V-PE Reagent (KGF003) was bought from KeyGEN Bio TECH, Nanjing, China. Sulfo Cy7-NHS ester and NH_2-alginate were bought from ruixi Biological Technology, China. SD rats and C57BL/6 mice of 3 months old were purchased from Nanjing

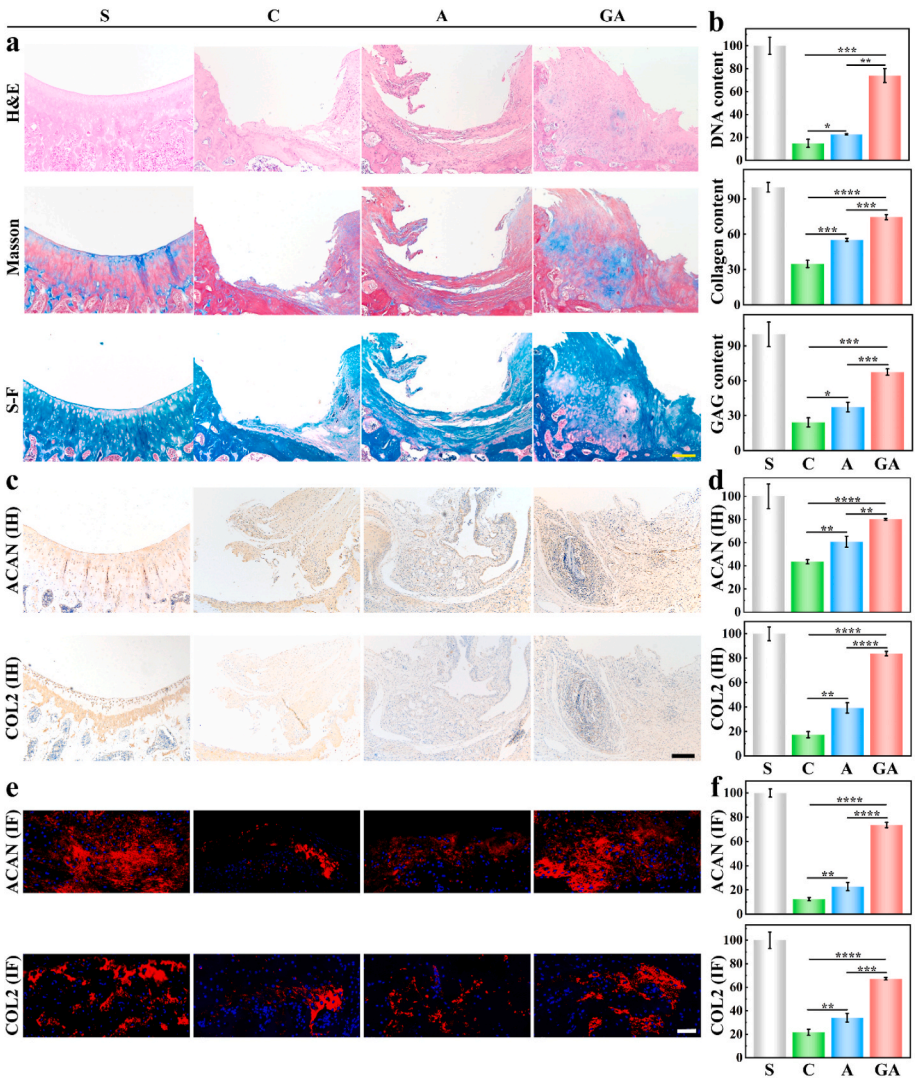

Fig. 7. (a–b), Representative H&E staining, Masson staining, and Safranin O-Fast Green staining (S–F), and their corresponding quantification of relative DNA content, relative collagen content, and relative GAG content (n = 3); (c–d) immunohistochemical staining of Aggrecan (ACAN) and collagen 2 (COL2), and their corresponding relative quantification (n = 3); (e–f) immunofluorescence staining of Aggrecan (ACAN) and collagen 2 (COL2), and their corresponding relative quantification (n = 3) at 3 months after implantation. The groups were S (sham), C (control), A (6% sodium alginate scaffold), and GA (15%/6% fish gelatin/sodium alginate scaffold). The yellow scale bar is 100 μm, and the white and black scale bars are 50 μm ($p < 0.05$).

University's Model Animal Research Center (Nanjing, China). The animals were treated in accordance the *Guide for the Care and Use of Laboratory Animals of the National Institutes of Health*, USA, and all surgical and perioperative procedures were conducted in accordance with the protocols of the Ethics Committee of Drum Tower Hospital, Medical School of Nanjing University (Nanjing, China). The ethics approval numbers were 2020AE01113 and 2020AE01119.

Preparation of hydrogels: Biomaterial inks of different ratios (% weight/volume) were prepared for further use in this study in the following combinations of fish skin gelatin and alginate: 0/6% (pure sodium alginate), 15/0% (pure fish skin gelatin), 15/3%, 15/6%, and 15/10%. The biomaterial inks were mixed according to the above ratios, added to the 5 ml serum-free 4% DMEM high glucose medium and were all stirred (80–120 rpm) for 2 h at 37 °C.

Characterization of viscosity and rheology: To investigate viscosity, the hydrogels were filled into glass bottles, placed at room temperature for 15 min, and turned upside-down to take photographs. The rheological properties of the biomaterial ink were tested with a Modular Advanced Rheometer System (Thermo Scientific HAAKE MARS, USA). A cone-plate with a diameter of 35 mm (P35/Ti 01170164) was used for the pure fish skin gelatin group, and a cylinder plate diameter with a diameter of 0.8 mm (P8/Ti 01181015) was used for other groups. The main parameters for testing were a truncation gap distance of 55 μm and a shear rate range of 0.01–100 s^{-1} at 37 °C.

3D printing of the biomaterial ink: Biomaterial inks were filled into the printing nozzle that sterilized with UV light and 75% ethanol, and homogenized for approximately 1–4 h at 4 °C for 3D printing. Modified 3D Bio-printer (Regenovo, China) and Bio-Architect WS (China) platforms were used to print models shaped in cylindrical and other shapes. The printing platform had provided many kinds of built-in models, and new models could be designed by 3D Builder. The influence of different ratios cold-water fish skin gelatin and sodium alginate, as well as various printing conditions such as air pressure, printing speed, and printing nozzles were tested using the controlling variate method.

Testing printability: A series of different % W/V ink compositions were chosen to make the mixed Sodium Alginate/Fish Gelatin biomaterial ink compositions and 3D printed one by one. The printing results were recorded according to the criteria of printable or nonprintable (whether the combination could be extruded out from the nuzzle smoothly), stable or unstable (whether the scaffold was stable at the room temperature for 3 min). It was liquid at the room temperature when the combination of Sodium Alginate/Fish Gelatin was thinner than 15/3%, thus, we also recorded them as nonprintable.

Crosslinking of the hydrogel scaffolds: The printed scaffolds were immersed into $CaCl_2$ (2% W/V) solution for physical crosslinking of sodium alginate for 3 min, and EDC/NHS (the mass concentration of EDC was 2 g/L, n_{EDC}: n_{NHS} = 4:1) solution to modify the gelatin for 30 min. And then, we washed the scaffolds with PBS for 3 times (5 min each time) to wash out extra solution, washed them with 75% ethanol for 3 times (5 min each time) and washed them with PBS once again.

Observation of the scaffolds: Stereomicroscope (OLYMPUS, SZX10, Japan) and Scanning electron microscope (SEM, S-4800, Hitachi, Japan) were used for gross and micro views of the scaffolds. These scaffolds were placed at −20 °C for 4 h before being freeze-dried by vacuum sublimation for 12 h. The surfaces of the scaffolds were then coated with gold to increase their conductivity before SEM observation.

Analysis of mechanical strength: In order to analyze the physical strength of the scaffolds, they were pruned into the shape of a cylinder (average parameters d = 4.0 mm h = 3.1 mm) and compressed at a constant speed of 1.0 mm/min. A tensile–compressive tester (Instron-5944 with a 2 kN sensor) applied force until the specimen broke, and all parameters were recorded automatically. Constant compressive strain curves were obtained, and their stress-strain and Young's modulus were calculated according to the Compressive Strain (Extension) Gauge Length Table and Stress-Strain Curve.

Immunogenicity and degradation: To study degradation, control (C), 15% pure cold-water fish skin gelatin biomaterial ink crosslinked with EDC/NHS (G), 6% sodium alginate 3D-printed scaffolds crosslinked with Ca^{2+} (A), and 15/6% fish gelatin/sodium alginate 3D-printed scaffolds also crosslinked with Ca^{2+} and EDC/NHS (GA) groups were prepared. The three groups of biomaterials were pruned into the same mass, sterilized with UV light and 75% ethanol for 24 h, and immersed into PBS several times before hypodermic implantation.

For immunogenicity, the biomaterials above were implanted under the skin of the mice (n = 4) for 2 weeks prior to H&E staining of the tissue derived from the implanted area and blood examination (regular blood test and blood chemistry analysis). Blood examination and H&E of the major organs such as the heart, liver, spleen, lungs, and kidneys were also carried out on the rats (n = 5) of the sham group (S), control group (C) and groups implanted with scaffolds (A, GA) to repair knee cartilage defects at 3 months.

For *in vitro* degradation analysis, the biomaterials above were put into a solution that contained 5 mU ml^{-1} alginate lyase (group A), Collagenase Type I (0.6 mg/ml) (group G) and both of these enzymes together (group GA), at 37 °C, pH = 7.40, for 2 weeks. The biomaterials were then washed with deionized water, dried at room temperature, and their weights were recorded to measure their degradation rate on days 0, 1, 3, 7, 9, 11, and 14.

For *in vivo* degradation analysis, Cy7 labeled fish skin gelatin and sodium alginate were prepared at first. To label fish skin gelatin with Cy7, fish skin gelatin and Cy7-NHS (Fish skin gelatin: Cy7-NHS = 1:1 mol) were added to a solution of 5 mL of 20 mmol/L carbonate buffer (pH 9.5). The solution was incubated with continuous stirring at 4 °C for 18 h in the dark. To label sodium alginate with Cy7, NH_2-alginate and Cy7-NHS (NH_2-alginate: Cy7-NHS = 1:1 mol) were added to a solution of 5 mL of 20 mmol/L carbonate buffer (pH 9.5). The solution was incubated with continuous stirring at 4 °C for 18 h in the dark to effect fluorescence and hypodermically implanted in the three groups of rats (n = 5) for 37 days. The fluorescence density of the implanted biomaterials was then tested on days 0, 7, 14, 21, 28, 35, and 37 using a small animal imaging system (Berthold, LB983 NC100, Germany).

Preparation of primary chondrocytes: Articular cartilage was extracted from the knee of 1-day-old rats. The extracted cartilage was cut into small pieces of about 1.0 mm^3 in size and digested with 0.2% type II collagenase in DMEM for 4 h at 37 °C, and the chondrocytes were cultured in 10% DMEM (including 10% fetal bovine serum and 1% penicillin-streptomycin) at 37 °C with 5% CO_2. The cells were then planted on the scaffolds in order to investigate cell proliferation.

Cell proliferation assay: The biocompatibility of the scaffolds was tested by seeding them with primary chondrocytes as mentioned above and C28 cells at a density of 7×10^4 cells/cm^2 and culturing at 37 °C with 5% CO_2 for 3–21 days. The viability of the chondrocytes on the scaffolds was also tested by Live and Dead Cell Viability Assay (Invitrogen, USA), confocal microscope (Nikon, A1RMP, Japan), Cell Counting Kit-8 (CCK-8; Dojindo, Japan), and optical density (OD) value at 450 nm according to the manufacturers' instructions.

Western blot analysis: For western blot analysis proteins were extracted from the C28 cells, separated by gel electrophoresis with 7.5–15% gels, and then transferred to nitrocellulose membranes. The Membranes were blocked for 1 h, incubated with primary antibodies (Aggrecan, SOX9, COL2A1, and Beta Actin) overnight at 4 °C, and washed with PBST 3 times. They were then incubated with respective secondary antibodies for 1 h and washed with PBST again. Finally, the protein bands were reacted with chemiluminescent substrate and imaged with a Tanon 5200 Multi Scanning System (Tanon, Shanghai, China).

RNA extraction, reverse transcription and real-time PCR: Total RNA from C28 cells was extracted using an RNA extracting kit (Abclonal, China) according to the manufacturer's instructions, and we also added 4 mL of the cDNA synthesis mix (Takara) to 1 mg RNA per sample according to the manufacturer's instructions for reverse transcription. RT-qPCR was performed on the ABI Viia 7 (Thermo) with SYBR Green-based detection system. The results were collected using the standard curve method and normalized to the GAPDH. The primer sequences used are shown in Table S1.

In vivo implantation: The SD Rats were randomly assigned (the same strain of rats, n = 5) into four groups. After first being anesthetized, the rats underwent aseptic preparations, a small incision was made at the knee, and the patella was dislocated to the lateral side to expose the knee joints. Next, full-thickness cartilage defects were created by penetrating into the subchondral bone at the femoral patellar groove on both knee joints of the left hind legs. For group S (sham), 2 rats were picked for sham surgery, and these animals only underwent an incision of the skin and exposure of the femoral patellar groove before closing the incision. For group C (control), knee joint cartilage defects were created, but nothing was implanted. Finally, for group A (6% sodium alginate scaffolds) and group GA (15/6% fish skin gelatin/sodium alginate scaffolds), the corresponding scaffolds were implanted into the defective areas, and the incision closed after the reduction of the patella. All procedures were performed by a single researcher, and all defects were uniformly drilled with the same electric drill with the same drilling bit to create a defect of 1.5 mm in depth and 2 mm in diameter.

Gross appearance: Three months after surgery, the 20 rats (20 knees) were euthanized, and some of the surrounding soft tissues of knee joints were removed in order to conduct MRI to investigate the amount of regenerated cartilage. Additionally, ICRS macroscopic evaluations were carried out on every knee with respect to gross appearance, degree of repair, integration condition, and macroscopic appearance of the surface. The ICRS assessments were carried out by three different investigators. Scoring Criteria from the ICRS Score for cartilage were given in Table S2.

Histological and immunohistochemical analysis: Regenerated cartilage was harvested to carry out histological, immunohistochemical and immunofluorescence analysis. HE, Safranin-O-Fast, and Masson staining were performed to evaluate the regeneration rate of the cartilage, glycosaminoglycan (GAG) deposition, and quantity of the repaired cartilage and collagen. Expression of collagen II and Aggrecan were examined by both Elisa and immunofluorescence analysis according to the manufacturer's protocols.

Statistical analysis: All quantitative data were expressed as mean ± standard deviation, and evaluated using the unpaired Student's t-test. All the experiments were performed 3 times unless otherwise stated, and all data were analyzed with SPSSAU24.0. A p-value <0.05 was used to indicate a statistically significant test result. Finally, we use the following notation: $*p < 0.05$, $**p < 0.01$, $***p < 0.001$, $****p < 0.0001$, and ns means no significance.

Ethics approval and consent to participate

The experimental protocol was established according to the ethical guidelines of the *Helsinki Declaration* and was approved by the *Ethics Committee of the Drum Tower Hospital*, Medical School of Nanjing

University. The ethics approval numbers were 2020AE01113 and 2020AE01119. And the animals were treated with the *Guide for the Care and Use of Laboratory Animals of the National Institutes of Health*, USA.

CRediT authorship contribution statement

Abudureheman Maihemuti: Investigation, Formal analysis, Software, Visualization, Data curation, Writing – original draft. **Han Zhang:** Writing – original draft, Writing – review & editing. **Xiang Lin:** Writing – review & editing. **Yangyufan Wang:** Software. **Zhihong Xu:** Methodology, Project administration, Supervision, Validation. **Dagan Zhang:** Conceptualization, Supervision, Validation, Writing – review & editing. **Qing Jiang:** Methodology, Project administration, Resources, Supervision, Funding acquisition.

Declaration of competing interest

The authors declare no competing financial interests and agreed to author contributions statements below.

Acknowledgments

This work was supported by the Key Program of NSFC (81730067), Major Project of NSFC (81991514), Jiangsu Provincial Key Medical Center Foundation, Jiangsu Provincial Medical Outstanding Talent Foundation, Jiangsu Provincial Medical Youth Talent Foundation, and Jiangsu Provincial Key Medical Talent Foundation. The Fundamental Research Funds for the Central Universities (14380493, 14380494), the National Natural Science Foundation of China (82102511), the Natural Science Foundation of Jiangsu (BK20210021), Research Project of Jiangsu Province Health Committee (M2021031).

The authors thank AiMi Academic Services (www.aimieditor.com) for English language editing and review services.

Appendix A. Supplementary data

Supplementary data to this article can be found online at https://doi.org/10.1016/j.bioactmat.2023.02.007.

References

[1] L. Sharma, N. Engl. J. Med. 384 (1) (2021) 51–59, https://doi.org/10.1056/NEJMcp1903768.
[2] X.D. Wu, D. Wu, W. Huang, G.X. Qiu, Ann. Rheum. Dis. 81 (7) (2022) E127, https://doi.org/10.1136/annrheumdis-2020-218433.
[3] Y. Xie, A. Zinkle, L. Chen, M. Mohammadi, Nat. Rev. Rheumatol. 16 (10) (2020) 547–564, https://doi.org/10.1038/s41584-020-0469-2.
[4] M. Li, H. Yin, Z. Yan, H. Li, J. Wu, Y. Wang, F. Wei, G. Tian, C. Ning, H. Li, C. Gao, L. Fu, S. Jiang, M. Chen, X. Sui, S. Liu, Z. Chen, Q. Guo, Acta Biomater. 140 (2022) 23–42, https://doi.org/10.1016/j.actbio.2021.12.006.
[5] A. Mahmoudian, L.S. Lohmander, A. Mobasheri, M. Englund, F.P. Luyten, Nat. Rev. Rheumatol. 17 (10) (2021) 621–632, https://doi.org/10.1038/s41584-021-00673-4.
[6] W. Wei, H. Dai, Bioact. Mater. 6 (12) (2021) 4830–4855, https://doi.org/10.1016/j.bioactmat.2021.05.011.
[7] H.P. Bei, P.M. Hung, H.L. Yeung, S. Wang, X. Zhao, Small (2021), https://doi.org/10.1002/smll.202101741.
[8] K.L. Bennell, K.L. Paterson, B.R. Metcalf, V. Duong, J. Eyles, J. Kasza, Y. Wang, F. Cicuttini, R. Buchbinder, A. Forbes, A. Harris, S.P. Yu, D. Connell, J. Linklater, B. H. Wang, W.M. Oo, D.J. Hunter, JAMA, J. Am. Med. Assoc. 326 (20) (2021) 2021–2030, https://doi.org/10.1001/jama.2021.19415.
[9] T.V. Pereira, P. Jueni, P. Saadat, D. Xing, L. Yao, P. Bobos, A. Agarwal, C. A. Hincapie, B.R. da Costa, BMJ Br. Med. J. (Clin. Res. Ed.) (2022) 378, https://doi.org/10.1136/bmj-2022-069722.
[10] Z. Wang, Y. Wang, J. Yan, K. Zhang, F. Lin, L. Xiang, L. Deng, Z. Guan, W. Cui, H. Zhang, Adv. Drug Deliv. Rev. 174 (2021) 504–534, https://doi.org/10.1016/j.addr.2021.05.007.
[11] Z. Zhou, J. Cui, S. Wu, Z. Geng, J. Su, Theranostics 12 (11) (2022) 5103–5124, https://doi.org/10.7150/thno.74548.
[12] N. Angel, S. Li, F. Yan, L. Kong, Trends Food Sci. Technol. 120 (2022) 308–324, https://doi.org/10.1016/j.tifs.2022.01.003.
[13] J. Chen, G. Zhang, Y. Zhao, M. Zhou, A. Zhong, J. Sun, Adv. Compos. Hybrid Mater. 5 (2) (2022) 1111–1125, https://doi.org/10.1007/s42114-022-00439-w.
[14] M. Rahmati, D.K. Mills, A.M. Urbanska, M.R. Saeb, J.R. Venugopal, S. Ramakrishna, M. Mozafari, Prog. Mater. Sci. (2021) 117, https://doi.org/10.1016/j.pmatsci.2020.100721.
[15] J. Coyne, N. Zhao, A. Olubode, M. Menon, Y. Wang, J. Contr. Release 318 (2020) 185–196, https://doi.org/10.1016/j.jconrel.2019.12.026.
[16] T. Jiang, J. Munguia-Lopez, S. Flores-Torres, J. Grant, S. Vijayakumar, A. De Leon-Rodriguez, J.M. Kinsella, JoVE 137 (2018), https://doi.org/10.3791/57826.
[17] K.F. Eichholz, F.E. Freeman, P. Pitacco, J. Nulty, D. Ahern, R. Burdis, D.C. Browe, O. Garcia, D.A. Hoey, D.J. Kelly, Biofabrication 14 (4) (2022), https://doi.org/10.1088/1758-5090/ac88a1.
[18] H. Cao, L. Duan, Y. Zhang, J. Cao, K. Zhang, Signal Transduct. Targeted Ther. 6 (1) (2021) 426, https://doi.org/10.1038/s41392-021-00830-x.
[19] N. Abbasi, S. Ivanovski, K. Gulati, R.M. Love, S. Hamlet, Biomater. Res. 24 (2020) 2, https://doi.org/10.1186/s40824-019-0180-z.
[20] S. Jin, J. Gao, R. Yang, C. Yuan, R. Wang, Q. Zou, Y. Zuo, M. Zhu, Y. Li, Y. Man, J. Li, Bioact. Mater. 8 (2022) 559–572, https://doi.org/10.1016/j.bioactmat.2021.06.028.
[21] F. Tao, Y. Cheng, X. Shi, H. Zheng, Y. Du, W. Xiang, H. Deng, Carbohydr. Polym. 230 (2020), https://doi.org/10.1016/j.carbpol.2019.115658.
[22] X. Zhang, L. Li, J. Ouyang, L. Zhang, J. Xue, H. Zhang, W. Tao, Nano Today 39 (2021), https://doi.org/10.1016/j.nantod.2021.101196.
[23] Y. Hu, H. Zhang, H. Wei, H. Cheng, J. Cai, X. Chen, L. Xia, H. Wang, R. Chai, Eng. Regenerat. 3 (2) (2022) 154–162, https://doi.org/10.1016/j.engreg.2022.04.001.
[24] L. Cai, C. Zhao, H. Chen, L. Fan, Y. Zhao, X. Qian, R. Chai, Adv. Sci. 9 (1) (2022), e2103384, https://doi.org/10.1002/advs.202103384.
[25] L. Yang, Y. Liu, L. Sun, C. Zhao, G. Chen, Y. Zhao, Nano-Micro Lett. 14 (1) (2021) 4, https://doi.org/10.1007/s40820-021-00747-8.
[26] L. Yang, L. Sun, H. Zhang, F. Bian, Y. Zhao, ACS Nano 15 (12) (2021) 20600–20606, https://doi.org/10.1021/acsnano.1c09325.
[27] Introduction, 3D Printing for Biomaterials 120 (19) (2020) 10545–10546, https://doi.org/10.1021/acs.chemrev.0c00139.
[28] C.M. Gonzalez-Henriquez, M.A. Sarabia-Vallejos, J. Rodriguez-Hernandez, Prog. Polym. Sci. 94 (2019) 57–116, https://doi.org/10.1016/j.progpolymsci.2019.03.001.
[29] W. Jung, Y.-H. Jung, P.V. Pikhitsa, J. Feng, Y. Yang, M. Kim, H.-Y. Tsai, T. Tanaka, J. Shin, K.-Y. Kim, H. Choi, J. Rho, M. Choi, Nature 592 (7852) (2021) 54, https://doi.org/10.1038/s41586-021-03353-1.
[30] G. Palmara, F. Frascella, I. Roppolo, A. Chiappone, A. Chiadò, Biosens. Bioelectron. 175 (2021), 112849, https://doi.org/10.1016/j.bios.2020.112849.
[31] K. Zub, S. Hoeppener, U.S. Schubert, Adv. Mater. 34 (31) (2022), https://doi.org/10.1002/adma.202105015.
[32] S. Vanae, M.S. Parizi, Engineered Regeneration 18 December 2020 2 (2021) 1–18, https://doi.org/10.1016/j.engreg.2020.12.001.
[33] T. Jiang, J.G. Munguia-Lopez, K. Gu, M.M. Bavoux, S. Flores-Torres, J. Kort-Mascort, J. Grant, S. Vijayakumar, A. De Leon-Rodriguez, A.J. Ehrlicher, J. M. Kinsella, Biofabrication 12 (1) (2019), 015024, https://doi.org/10.1088/1758-5090/ab3a5c.
[34] G. Chen, X. Liang, P. Zhang, S. Lin, C. Cai, Z. Yu, J. Liu, Adv. Funct. Mater. 32 (34) (2022), https://doi.org/10.1002/adfm.202113262.
[35] M. Dong, Y. Han, X.P. Hao, H.C. Yu, J. Yin, M. Du, Q. Zheng, Z.L. Wu, Adv. Mater. 34 (34) (2022), https://doi.org/10.1002/adma.202204333.
[36] M. Ryma, H. Genç, A. Nadernezhad, I. Paulus, D. Schneidereit, O. Friedrich, K. Andelovic, S. Lyer, C. Alexiou, I. Cicha, J. Groll, Adv. Mater. 34 (28) (2022), https://doi.org/10.1002/adma.202200653.
[37] M.A.S.R. Saadi, A. Maguire, N.T. Pottackal, M.S.H. Thakur, M.M. Ikram, A.J. Hart, P.M. Ajayan, M.M. Rahman, Adv. Mater. 34 (28) (2022), https://doi.org/10.1002/adma.202108855.
[38] Q. Zhang, Z. Xu, X. Zhang, C. Liu, R. Yang, Y. Sun, Y. Zhang, W. Liu, Adv. Funct. Mater. 32 (23) (2022), https://doi.org/10.1002/adfm.202200360.
[39] X. Wang, C. Yang, Y. Yu, Y. Zhao, Research 2022 (2022), 9794745, https://doi.org/10.34133/2022/9794745.
[40] C.F. Guimarães, R. Ahmed, A.P. Marques, R.L. Reis, U. Demirci, Adv. Mater. 33 (23) (2021), e2006582, https://doi.org/10.1002/adma.202006582.
[41] Y. Hu, Z. Chen, H. Wang, J. Guo, J. Cai, X. Chen, H. Wei, J. Qi, Q. Wang, H. Liu, Y. Zhao, R. Chai, ACS Nano 16 (2) (2022) 1868–1879, https://doi.org/10.1021/acsnano.1c11627.
[42] Y. Liu, L. Sun, H. Zhang, L. Shang, Y. Zhao, Chem. Rev. 121 (13) (2021) 7468–7529, https://doi.org/10.1021/acs.chemrev.0c01289.
[43] Z. Zhao, G. Li, H. Ruan, K. Chen, Z. Cai, G. Lu, R. Li, L. Deng, M. Cai, W. Cui, ACS Nano (2021), https://doi.org/10.1021/acsnano.1c02147.
[44] M. Amiri, P. Khazaeli, A. Salehabadi, M. Salavati-Niasari, Adv. Colloid Interface Sci. 288 (2021), 102316, https://doi.org/10.1016/j.cis.2020.102316.
[45] S. Liu, Y.N. Wang, B. Ma, J. Shao, H. Liu, S. Ge, ACS Appl. Mater. Interfaces 13 (31) (2021) 36880–36893, https://doi.org/10.1021/acsami.1c08855.
[46] G. Luo, Y. Sun, J. Zhang, Z. Xu, W. Lu, H. Wang, Y. Zhang, H. Li, Z. Mao, S. Ye, B. Cheng, X. Fang, Theranostics 11 (8) (2021) 3642–3660, https://doi.org/10.7150/thno.53089.
[47] Y. Jiang, H. Zhang, J. Wang, Y. Liu, T. Luo, H. Hua, J. Hematol. Oncol. 15 (1) (2022) 34, https://doi.org/10.1186/s13045-022-01252-0.
[48] N.K. Karamanos, Z. Piperigkou, A. Passi, M. Götte, P. Rousselle, I. Vlodavsky, Trends Mol. Med. 27 (10) (2021) 1000–1013, https://doi.org/10.1016/j.molmed.2021.07.009.

[49] W. Ahn, J.H. Lee, S.R. Kim, J. Lee, E.J. Lee, J. Mater. Chem. B 9 (8) (2021) 1919–1940, https://doi.org/10.1039/d0tb02604b.
[50] M. Filippi, G. Born, M. Chaaban, A. Scherberich, Front. Bioeng. Biotechnol. 8 (2020) 474, https://doi.org/10.3389/fbioe.2020.00474.
[51] C. Zhao, L. Hu, C. Zhang, S. Wang, X. Wang, Z. Huo, Environ. Pollut. 287 (2021), 117303, https://doi.org/10.1016/j.envpol.2021.117303.